THE JOURNAL OF PHYSICAL CHEMISTRY C

Article

pubs.acs.org/JPCC

Adsorption of NH_3 with Different Coverages on Single-Walled ZnO Nanotube: DFT and QTAIM Study

Naiara L. Marana,[†] Silvia M. Casassa,[‡] and Julio R. Sambrano[†,*]

[†]Modeling and Molecular Simulations Group, São Paulo State University, UNESP, 17033-360 Bauru, São Paulo, Brazil

[‡]Theoretical Group of Chemistry, Chemistry Department I.F.M., Torino University, Torino 10124, Italy

Supporting Information

ABSTRACT: NH_3 adsorption with different coverages on single-walled armchair and zigzag ZnO nanotubes (ZnONT) has been studied via periodic computational simulations at the all-electron B3LYP level. In order to fully characterize the molecules-surface interaction, infrared (IR) spectra were calculated for the first time. A rigorous analysis of the electron density in the bonding region, according to the quantum theory of atoms in molecules, was performed. NH_3 molecules physisorb without dissociation via a self-catalyzed process. Although the nanotubes undergo sensitive lattice deformations with low coverages, its fundamental electronic properties were not modified. Owing to these analyses, the ZnONTs can be applicable as NH_3 gas sensor.

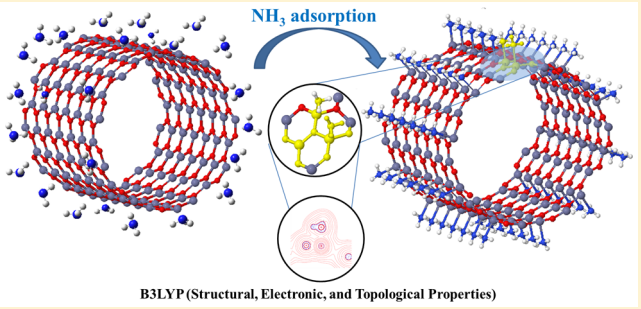

INTRODUCTION

Zinc oxide (ZnO) wurtzite is a well-recognized multifunctional material with a direct band gap energy (3.37 eV)[1] and with several technological applications due to the low cost of synthesis, chemical stability, and nontoxicity.[2,3]

In recent years, among other uses, ZnO-based structures applied as gas sensors have been the subject of several research. Catto et al.[4] reported a low-temperature method to prepare an ozone gas sensor based on hexagonal one-dimensional (1D) ZnO nanorod-like structure via a hydrothermal process. ZnO nanostructures with sensitivity toward low O_3 concentrations, as well as good stability, fast response, and short recovery time, has been recently reported by Rocha et al.[5]

An experimental study by Biasotto and co-workers[6] exploited the considerable surface-to-volume ratio and porous sensitivity of ZnO films to design devices for CO gas detection. Wang and co-workers[7] studied the response and viability of ZnO nanorod to detect NO_2 in the presence of several critical influencing factors and have found rather good performances in sensitivity and response speed. ZnO nanorods-based ammonia sensors, with a cross-linked configuration structures, as reported by Chen et al.,[8] exhibit effective capability in detecting ammonia at a concentration of 10 ppm NH_3/air.

Due to its high specific area, fine particle size, and quantum confinement properties, ZnO nanowires are believed to represent promising candidates for gas sensing applications[9] in particular as regards to ammonia detection.[10] However, a few theoretical papers are devoted to study the characteristics and implications of gas molecules interaction with 1D ZnO structures. An et al.[11] investigated the electronic and structural properties of a single-walled ZnO nanotube (6, 0) as a potential sensor for O_2, H_2, NH_3, and NO_2. Their density functional theory (DFT) calculations showed that molecules are mainly chemisorbed and that CO and ammonia behaves as charge donors enhancing the electron concentration of ZnO.

Among several gaseous molecules, the present study focus is on ammonia (NH_3) adsorption. This molecule is extensively applied in many areas, such as food, pharmaceutical, chemical industries and medical diagnoses, among others. Nevertheless, ammonia is a toxic gas and a severe irritant to the respiratory tract. An exposure over 15 min needs to be limited to 25−35 ppm, and the time-weighted-average over an 8 h period should not exceed 25 ppm. Depending on those conditions and sensibilities, the critical need of reliable and effective ammonia monitoring everywhere is urgent,[12] which implies the need to develop more efficient materials for detection.

Many ammonia sensors are already based on pure ZnO bulk phases and surfaces.[13−15] Nonetheless, ZnO nanostructures could represent an improvement in gas sensor technology due to their large specific surface area, and as far as we know, there is no experimental evidence with respect to the experimental NH_3 adsorption on ZnO nanotubes. Therefore, computational simulations can give indications of the adsorption mode and give subsidies for future experimental works.

This paper reports DFT periodic simulations performed at the B3LYP hybrid functional/all-electron basis set level to investigate the structural and electronic properties of NH_3

Received: October 14, 2016
Revised: March 11, 2017
Published: March 14, 2017

DOI: 10.1021/acs.jpcc.6b10396
J. Phys. Chem. C 2017, 121, 8109−8119

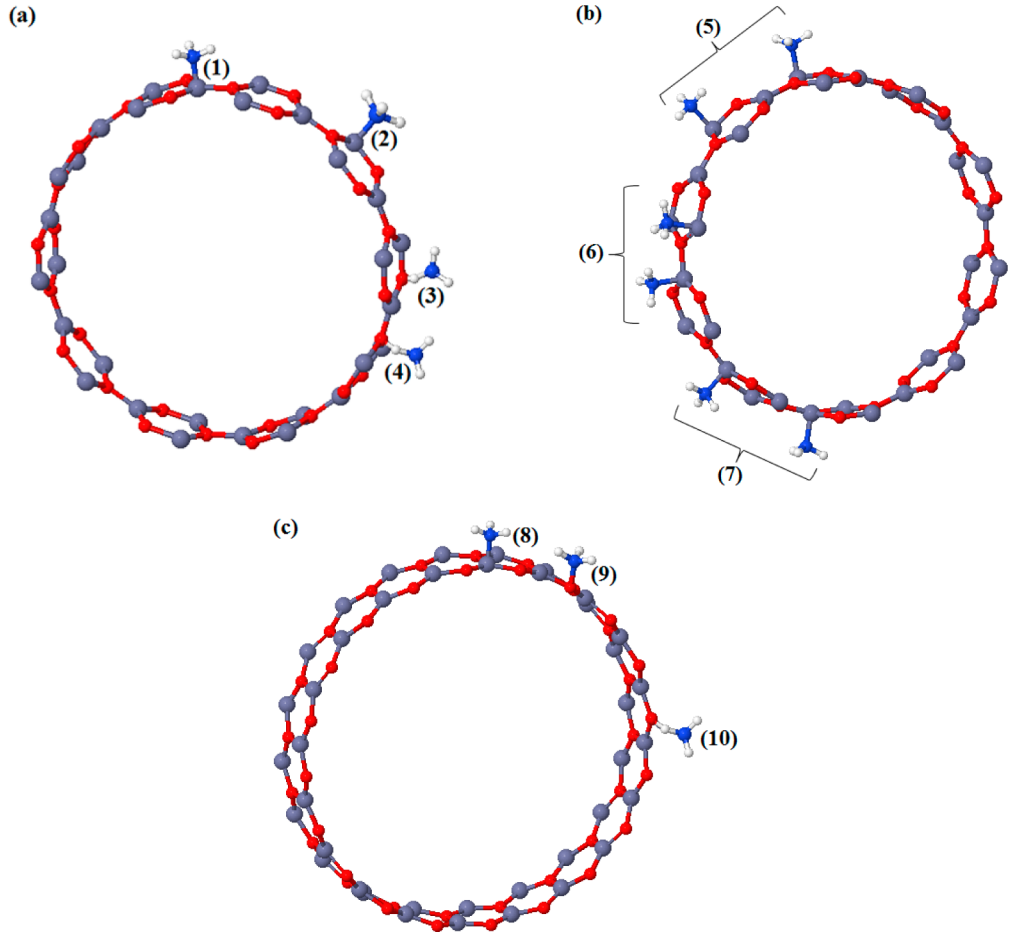

Figure 1. NH_3 adsorption on various surface sites and with different coverages on (a) armchair: (1) Model A: Zn_{Ax}−NH_3, (2) Model B: Zn_{Eq}−NH_3, (3) Model C: O−HNH_2, (4) Model D: O−HNH_2; (b) simultaneous adsorption: (5) both Zn_{Eq}, (6) Zn_{Eq} and Zn_{Ax}, (7) both Zn_{Ax}; and (c) zigzag: (8) Model E: Zn−NH_3, (9) Model F: O−HNH_2, and (10) Model G: O−HNH_2.

adsorption on armchair (10, 10) and zigzag (20, 0) single-walled ZnO nanotubes (*n*NH3@ZnONT). Adsorption energies as a function of the surface coverage are calculated, and the influence of the NH_3 adsorption on structural and electronic properties of ZnONTs is analyzed. In order to fully characterize the molecules−surface interaction, infrared (IR) spectra were calculated, and a rigorous analysis of the electron density in the bonding region according to the quantum theory of atoms in molecules (QTAIM)[16] was accomplished.

THEORETICAL METHODS

The computational simulations were performed using the CRYSTAL14[17] program which solves the Schrodinger equation for periodic systems in one, two, and three dimensions in a basis set of localized atomic orbitals. Similar to the majority of the available studies of our research group,[18−20] this paper is based on DFT calculations with the standard B3LYP hybrid functional.[21−23] The choice of the B3LYP functional is based on the comparison of previous results obtained with the HSE06 and B3LYP-D3 functional, which consider dispersive energies. However, the results obtained with HSE06 and B3LYP-D3 are close to those obtained with the standard B3LYP functional. Therefore, it was decided to use the standard B3LYP functional due to the great description of ZnO properties and the low computational cost. Zinc, oxygen, nitrogen, and hydrogen atoms were described by 86−411d31G,[24] 8−411d1,[25] 6−21G*,[26] and 5−11G*[27] all-electron basis set, respectively. The accuracy of the truncation criteria for bielectronic integrals is controlled by a set of five thresholds whose values have been set to 10^{-10}, 10^{-10}, 10^{-10}, 10^{-20}, and 10^{-40}. In the self-consistent field procedure (SCF), the shrinking factor for both the Fock matrix diagonalization and the energy calculation was set to 4, corresponding to 3 independent k-points in the irreducible part of the Brillouin zone. Basins integration to estimate atomic Bader charges was performed on a 120 × 96 × 120 grid of points in the direct space.[28] The vibrational frequencies at the Γ point were computed within the harmonic approximation by diagonalizing the mass-weighted Hessian matrix.[29,30]

The following step-by-step strategy has been adopted to simulate NH_3 adsorption on ZnONTs. First, the wurtzite ZnO bulk structure has been optimized relaxing both the lattice parameters (*a* and *c*) and internal coordinate, *u*. Then, the (0001) monolayer was cut out from the bulk, and a new optimization of the internal coordinates of the (0001) surface was performed. Finally, by rolling the (0001) relaxed monolayer surface,[17,23,31−33] we obtained the 40 atoms unit cell (10, 10) armchair nanotube and the 80 atoms unit cell (20, 0) zigzag nanotube, both characterized by a diameter of ∼20 Å, and cylinder axes (|*l*|) of 3.28 and 5.67 Å, respectively. In a previous works,[32,33] these structures were designed as

DOI: 10.1021/acs.jpcc.6b10396
J. Phys. Chem. C 2017, 121, 8109−8119

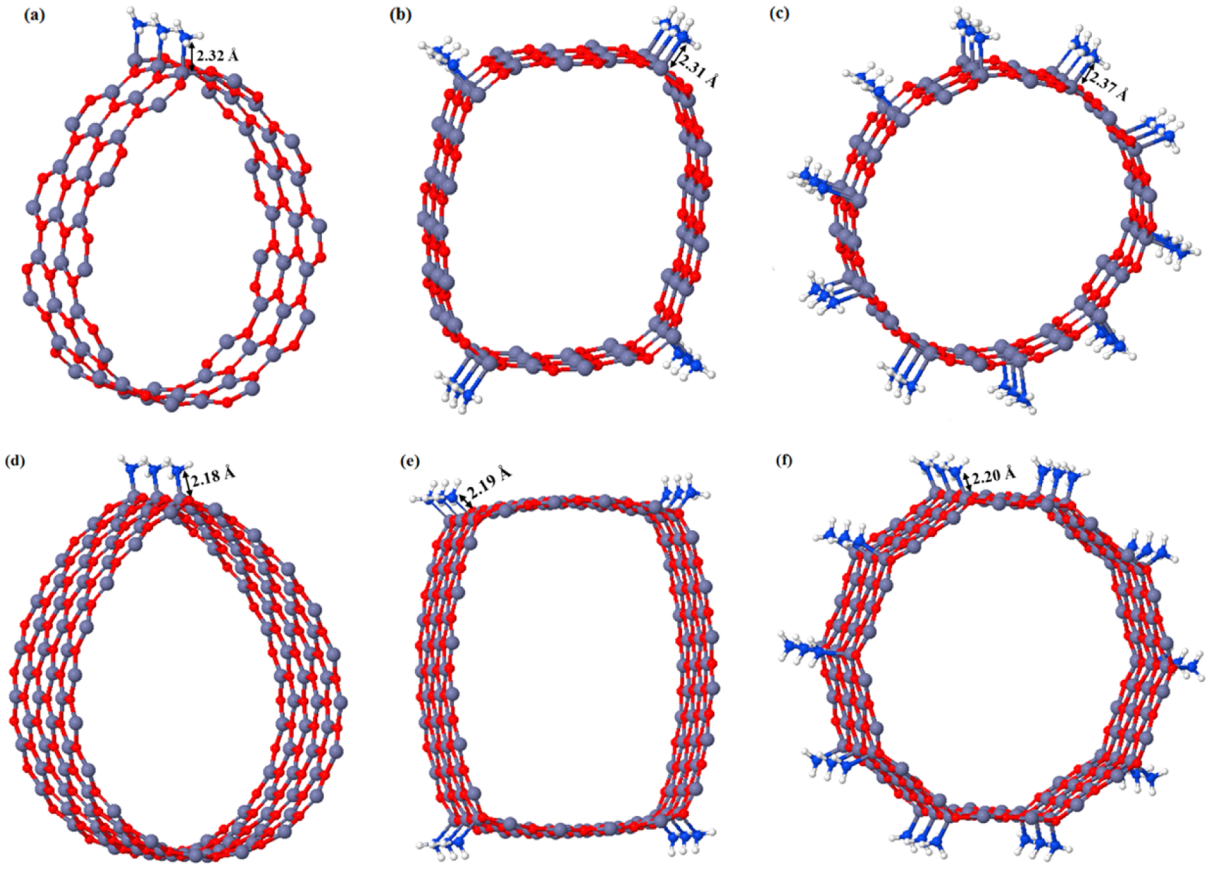

Figure 2. Nanotube deformation after NH_3 adsorption and optimization. Armchair: (a) 1-row of NH_3 molecules, (b) 4-rows, and (c) 10-rows; zigzag: (d) 1-row, (e) 2-row, and (f) 10-rows of NH_3.

an ideal model to perform adsorption studies thanks to its minimum energy formation and strain.

In DFT simulation, in absence of any dynamic and thermal effects, the final configuration of an adsorbate is significantly influenced by its initial position. In order to explore all the possibilities and to individuate the adsorption sites and the optimum coverage, several different starting configurations were investigated. With reference to Figure 1, four adsorption sites were considered on the armchair ZnONT surface: the axial and equatorial positions of Zn atom (Figure 1a, sites 1 and 2) and of O atom (Figure 1a, sites 3 and 4), respectively. For each adsorption site, two different molecular approaches were performed: via nitrogen atom (Figure 1a, sites 1 and 2) and via hydrogen atom (Figure 1a, sites 3 and 4). However, in the zigzag nanotube case, all adsorption sites are equivalent; therefore, only NH_3 approaches were performed (Figure 1c). It is important to emphasize that the periodicity along one direction is preserved, so all the configurations represent the adsorption of an infinite row of NH_3 molecules along the ZnO *x*-direction (see Figure 2). This corresponds to 1 NH_3 per unit cell. To model the single-molecule dilution limit, a supercell calculation was carried out on a unit containing 160 and 240 atoms for armchair and zigzag, respectively, and only 1 NH_3 molecule.

As the equilibrium configuration of a single row of NH_3 was identified, we considered the possibility of ammonia molecules adsorbed in neighboring positions. Three possibilities were envisaged: both molecules on equatorial (Figures 1b, site 5) or axial sites (Figure 1b, site 7) or one ammonia in the axial and the other in the equatorial position (Figure 1b, site 6). The most stable among these geometries was repeated with NH_3 rows going from 2 up to the saturation limit of 10, as represented in Figure 2.

The adsorption energy was calculated according to the expression

$$E_{\mathrm{ads}/N} = \frac{1}{N}[E_{(\mathrm{NT})+\mathrm{NH}_3} - (E_{(\mathrm{NT})} + NE_{\mathrm{NH}_3}) + E_{\mathrm{BSSE}}] \quad (1)$$

where $E_{(\mathrm{NT})+\mathrm{NH}_3}$ is the total energy of the optimized nanotube with adsorbed NH_3 molecule, $E_{(\mathrm{NT})}$ is the total energy of the isolated optimized nanotube, N is the number of adsorbed NH_3 molecules per unit cell, and E_{NH_3} is the total energy of ammonia in gas phase. E_{BSSE} is the correction energy due to the basis set superposition error (BSSE).[34] Calculations performed with localized basis sets are susceptible to this error, which occurs when atoms belonging to different interacting moieties approach each other and the overlap among their basis functions produces a spurious stabilization that is inversely proportional to the quality of the adopted basis set. There are two ways to estimate the BSSE, the *a priori* chemical Hamiltonian approach (CHA)[35] and the *a posteriori* counterpoise method (CP);[34] although conceptually different, the two approaches tend to give similar results. In this work, the CP correction was applied to all the energies as follows:

$$E_{\mathrm{BSSE}} = (E_{(\mathrm{NT})}^{\mathrm{frozen}} - E_{(\mathrm{NT})+\mathrm{ghost}}^{\mathrm{frozen}}) + (E_{\mathrm{NH}_3}^{\mathrm{frozen}} - E_{\mathrm{ghost}+\mathrm{NH}_3}^{\mathrm{frozen}}) \quad (2)$$

DOI: 10.1021/acs.jpcc.6b10396
J. Phys. Chem. C 2017, 121, 8109−8119

Table 1. Zn−O, N−H, and Zn−N Bond Lengths (Å), Zn−O−Zn and H−N−H Bond Angles (deg), Distortion Energy (E_{dist}) and Adsorption Energy (E_{ads}) (kJ/mol), and Band Gap (E_{gap}, eV) of *n*NH3@ZnONT[a]

nNH$_3$	d_{Zn-O}	$d_{s(Zn-O)}$	$\alpha_{Zn-O-Zn}$	$\alpha_{sZn-O-Zn}$	d_{Zn-N}	d_{N-H}	α_{H-N-H}	E_{dist}	E_{ads}	E_{ads} + E_{BSSE}	E_{gap}
Armchair											
0	1.89	1.89	119.79	119.79				0.00			4.52
1	1.89	1.93	119.88	116.12	2.32	1.02	107.49	14.02	−70.17	−18.66	4.18
1-row	1.91	1.94	119.74	117.88	2.32	1.02	103.02	10.25	−40.59	−22.85	4.36
2-row	1.90	1.94	119.64	117.87	2.30	1.02	107.35	22.55	−60.17	−20.71	4.43
4-row	1.90	1.94	119.87	118.17	2.31	1.02	107.30	15.56	−66.07	−26.90	4.38
5-row	1.90	1.94	119.90	118.28	2.33	1.02	106.40	14.64	−66.27	−27.11	4.37
10-row	1.90	1.93	119.90	118.93	2.37	1.02	106.33	8.95	−64.68	−26.40	4.22
Zigzag											
0	1.89	1.89	119.90	119.90				0.00			4.53
1	1.89	1.94	119.80	119.70	2.17	1.02	107.24	89.58	66.13	39.94	4.47
1-row	1.89	1.96	119.91	113.20	2.18	1.02	107.40	82.92	−29.43	25.20	4.43
2-row	1.89	1.96	118.23	114.39	2.18	1.02	107.40	57.29	−57.18	−2.50	4.46
4-row	1.89	1.95	119.95	114.55	2.19	1.02	107.41	44.70	−68.64	−13.39	4.44
5-row	1.89	1.95	119.98	114.66	2.19	1.02	107.44	42.06	−70.38	−14.90	4.43
10-row	1.89	1.95	119.98	119.96	2.20	1.02	107.45	34.52	−77.45	−15.74	4.40
6 (6, 0)[11]	1.94				2.16				−78.91		2.25
1 (0001)[37]					2.04				−213.00		
1 (10$\bar{1}$0)[36]					2.06	1.02	107.00		−146.00		
1 (10$\bar{1}$0)[39]					2.06	1.01			−175.81		

[a]The sub-index s refers to the atoms of the adsorption site.

where all the energies refer to the geometries of the two separated moieties frozen in the minimum adsorption configuration, with and without ghost functions, respectively.

The distortion energy, E_{dist}, due to the structural modifications of the ZnONTs lattice which occur as one of the main effects of the adsorption process, was evaluated according to the following equation:

$$E_{dist/N} = \frac{1}{N}(E_{(NT)}^{frozen} - E_{(NT)}) \quad (3)$$

In order to estimate the heat of adsorption and its temperature dependency, the enthalpy of each moiety was calculated at 0 and 298 K as follows:

$$H(T) = E_L + E_0 + PV + E_T \quad (4)$$

where E_L is the electronic term, E_0 and E_T are the zero-point and temperature-dependent contributions to the vibrational energy, respectively, and PV is the pressure per volume contribution.

Finally, the ZnONT−NH$_3$ interactions were characterized by exploiting the potentiality of Bader topological analysis of the electron density, as implemented in the TOPOND program[28] incorporated in the CRYSTAL14 package. Bader charges were computed to estimate the amount and direction of the charge transfer between the NH$_3$ and the ZnONTs. A complete search of the bond critical points (BCP) between the adsorbates and the nanotubes has been carried out, and their topology has been fully characterized to shed light on the bonding nature. Moreover, the sensitiveness of these indicators has allowed us to follow the effects of the adsorption and coverage on the Zn−O bonds.

RESULTS AND DISCUSSION

Previous accurate studies on the structural, electronic, and vibrational properties of ZnO bulk, (0001) monolayer surface, and bare armchair and zigzag nanotubes can be found in refs 32 and33. Ammonia adsorption has then been modeled on the fully characterized ZnONTs.

Table 2. Adsorption Energies and Enthalpies at 0 and 298 K (kJ/mol)

nNH$_3$	E_{ads} + E_{BSSE}	H_{ads} (0 K)	H_{ads} (298 K)
Armchair			
1-row	−22.85	−13.81	−11.88
4-row	−26.90	−17.99	−17.62
10-row	−26.40	−18.03	−17.91
Zigzag			
1-row	25.20	30.00	38.53
4-row	−13.40	−3.07	−2.47
10-row	−15.74	−5.90	−4.53

On the basis of preliminary investigation on the different sites, it was confirmed that NH$_3$ adsorption takes place via nitrogen on the Zn atom. In armchair nanotube, the most stable configuration is the NH$_3$ adsorption on Zn axial atom. The overall energy cost, which takes into account both the N−Zn bond formation and the nanotube relaxation, is about 33.0 and 62.8 kJ/mol lower than that on the other sites, whose optimized geometries are reported in Figure S1.

The results are summarized in Table 1, with the adsorption occurring by an equilibrium distance of 2.30 and 2.17 Å, for armchair and zigzag nanotubes, respectively. The adsorption energies of NH$_3$ calculated with the supercell approach are −18.66 and 39.94 kJ/mol, for armchair and zigzag nanotubes, respectively, which represent our model for isolated ammonia interacting with ZnONTs. As far as a single row of NH$_3$ is considered, the adsorption energies decrease, and the difference between these values is a good estimate of the interaction which takes place between nearby adsorbed molecules and the nanotube surface. For what concerns the adsorption geometry, NH$_3$ almost preserves its gas-phase structure. On armchair nanotube, the H point is far from the nanotube surface and does not interact with the underlying oxygen atoms. In contrast, on zigzag

DOI: 10.1021/acs.jpcc.6b10396
J. Phys. Chem. C 2017, 121, 8109−8119

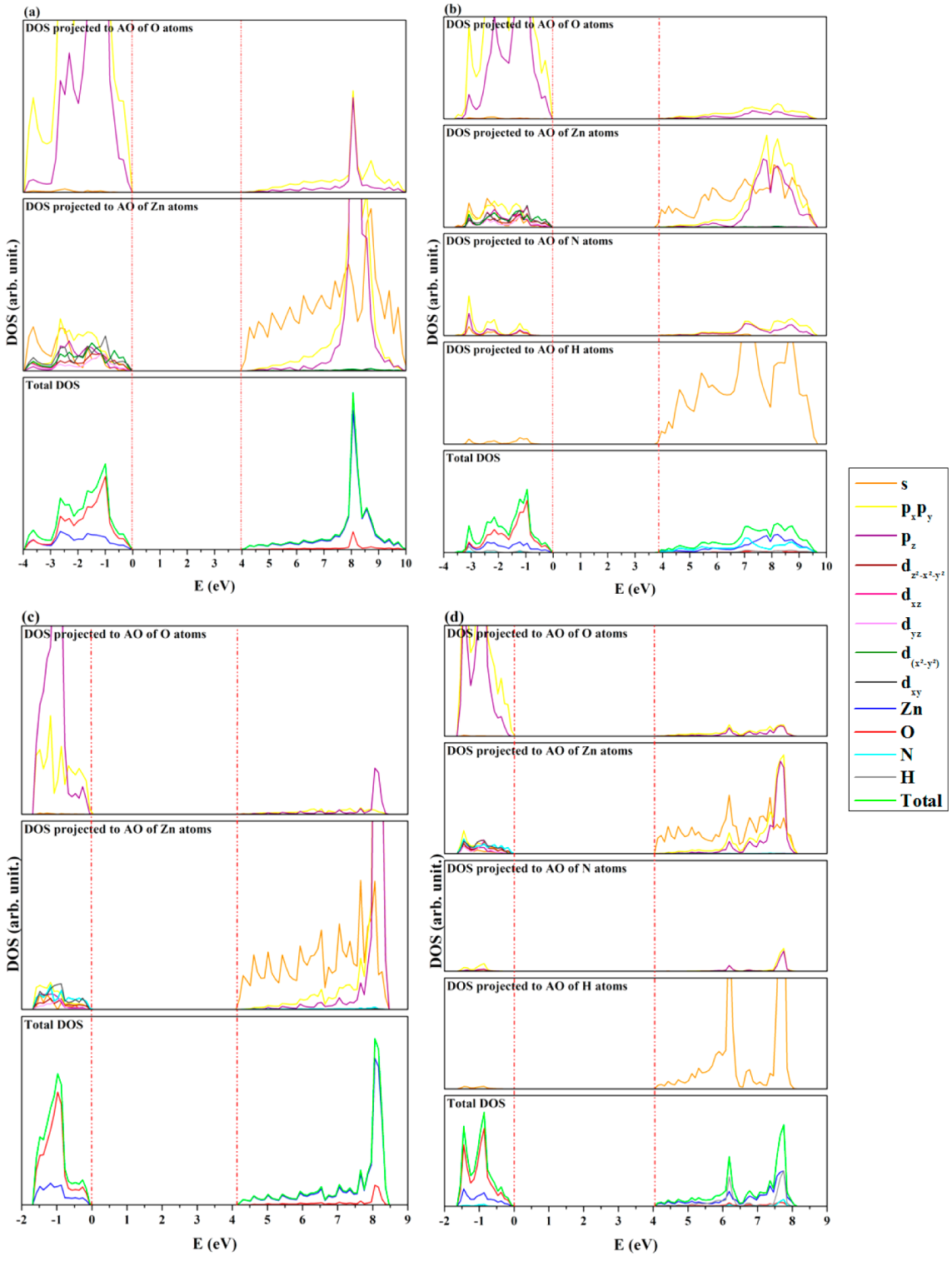

Figure 3. Density of states of (10, 10) nanotube (a) bare and (b) with 10-rows of NH_3 molecules adsorbed and (20, 0) nanotube (c) bare and (d) with 10-rows of NH_3 molecules adsorbed.

nanotube, the ammonia hydrogen interacts with the O of nanotube surface, as shown in more details in topological analysis. The nanotube surface atoms involved in the process show a sensitive elongation of their bond length and shrinkage of the angles. Oxygen and Zn atoms belonging to the other hexagons are almost unaffected by NH_3 uptake, indicating that the interaction is rather localized although effective. In fact, the values of E_{dist} are not negligible with a maximum strain suffered by the $2NH_3$@ZnONT and $1NH_3$@ZnONT systems, for armchair and zigzag nanotubes, respectively, which are visibly stretched along the Zn−NH_3 direction and a minimum for the symmetric $10NH_3$@ZnONT coverage.

As a general comment, the adsorption energies are sensitively lower than those evaluated by others authors on similar systems.[11,36−39] Indeed, there are many reasons to explain these differences. First, most of the calculated binding energies do not

DOI: 10.1021/acs.jpcc.6b10396
J. Phys. Chem. C 2017, 121, 8109−8119

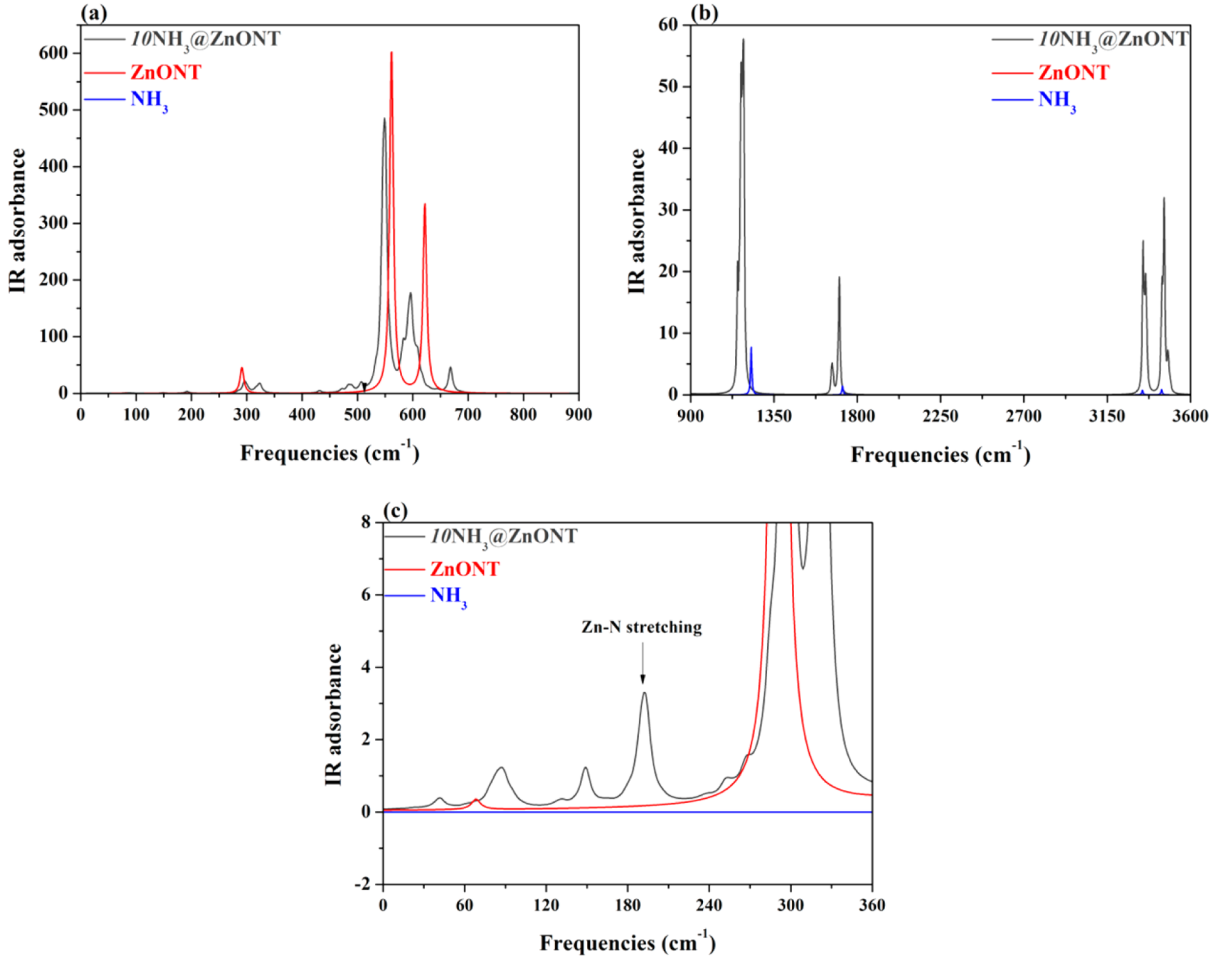

Figure 4. Infrared spectra of NH_3 adsorption on armchair ZnONT in the (a) low- and (b) high-frequency range. (c) Zoom-in view of the peaks corresponding to the Zn−N stretching modes.

take into account the BSSE. Our BSSE's are on order of 38.0 and 55.0 kJ/mol, for armchair and zigzag nanotubes, respectively, values that if neglected would yield results in better agreement with literature and in the meantime would lead to incorrect conclusions. This difference between BSSE is mostly due to interaction between ammonia H and O of zigzag nanotube, which leads to a higher BSSE and E_{ads}. Moreover, in literature the adsorption of a single NH_3 on a surface was modeled, and the effects of different coverage were not taken into account. Then, as can be seen in Figure 2 (and in Figures S3 and S4) and has been already commented on, the interaction with ammonia induces evident deformations on the soft nanotube lattice, estimated to be on the order of 8−14 and 34−89 kJ/mol, for armchair and zigzag nanotubes, respectively, strains that are totally absent in the case of extended surfaces. Finally, some surfaces present a complete different topology, and this is the case of the $(10\bar{1}0)$ layer where both the Zn and the O atoms are exposed and can easily interact with the incoming molecule.[36,39]

In order to take into account the effect of the nuclear motion on the surface processes, the heats of adsorption were calculated at 0 and 298 K and reported in Table 2. On zigzag nanotube, the adsorption process is promoted by the increase of NH_3 molecules adsorbed, which is an endothermic process in $1NH_3$@ZnONT. In all other models, NH_3 physisorption occurs as an exothermic process only slightly affected by an increase of the temperature.

The adsorption of the NH_3 molecules leads to a small reduction of E_{gap}. Qualitatively, it is difficult to distinguish very close values, especially from an experimental point of view, although there are experiments related to structural disorders that lead to small changes in the band gap.[40] Therefore, despite the difficulties, we highlighted the small differences found in order to call attention for possible experimental research. In the armchair case, the 2-row presents the most E_{dist}, which leads to a higher E_{gap}. However, on zigzag nanotube, the most pronounced E_{gap} also occurs on $2NH_3$@ZnONT, if it is considered that the effective adsorption occurs from this model (since in this model the adsorption energies become negative, and it consequently shows that there is an adsorption and not just an interaction, as in one single NH_3 and 1-row models). In this sense, the reduction is more pronounced with saturation of NH_3, i.e., $10NH_3$@ZnONT molecules. The nanotube armchair presents a reduction of 0.30 eV, whereas for the zigzag, it is 0.13 eV. This difference may be due not only to the greater distortions suffered by the zigzag nanotube but also the presence of van de Waals interactions.

In order to investigate the electronic structure of these heterogeneous systems, the bands structure and density of states of $10NH_3$@ZnONT with bare nanotubes were compared. As can be seen in Figure S5, the physisorption keeps the bands main features unchanged. However, as already said, some effects can be perceived on the band gap which undergoes a small but sensitive reduction due to the upper shift of the occupied 3d

DOI: 10.1021/acs.jpcc.6b10396
J. Phys. Chem. C 2017, 121, 8109−8119

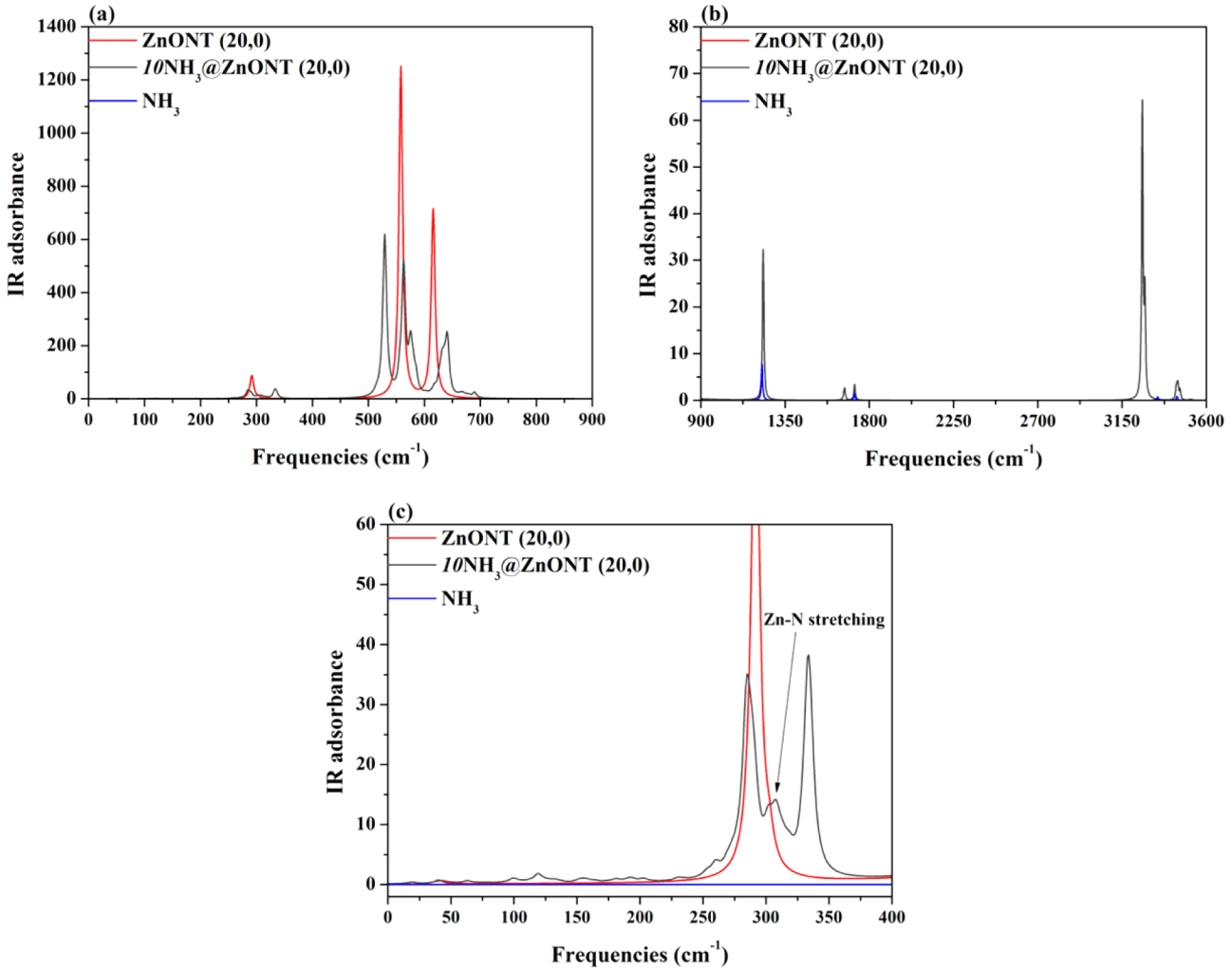

Figure 5. Infrared spectra of NH_3 adsorption on zigzag ZnONT in the (a) low- and (b) high-frequency range. (c) Zoom-in of the peaks corresponding to the Zn−N stretching modes.

orbitals of the Zn atom. In particular, the $3d_{(x^2-y^2)}$ and $3d_{xy}$ orbitals are shifted higher in energy with respect to the others; see Figure 3. At the conduction band, ∼9.0 eV, the p orbitals of zinc atoms maintain the contribution, while the 2p orbitals of oxygen atoms decrease the contribution after adsorption. With respect to the NH_3 molecules, the contribution of nitrogen is most intense in the valence band when adsorbed by armchair nanotube, while in zigzag nanotube, the contribution is most intense at the inner conduction band. The hydrogen contributes more in the conduction band. The $2p_xp_y$ orbital of nitrogen atoms contributes more over the entire range examined, and the s and $2p_z$ orbitals presents almost the same contribution.

With the aim to see the influence of NH_3 molecules on ZnONTs frequencies, the IR spectra of *10*NH_3@ZnONT of armchair and zigzag nanotubes (Figure 4 and 5) were calculated. For sake of clarity, the spectra were subdivided into two parts, the low (0−900 cm^{-1}) and high (900−3600 cm^{-1}) frequencies regions. Signals of the isolated ZnONTs and of the gas-phase NH_3 molecule are superimposed for the sake of comparison.

ZnONTs vibrate according to modes with frequencies below 700 cm^{-1}. As the adsorption takes place, peaks at about 550 cm^{-1}, mainly due to oxygen displacements,[33] are split into several signals. Then, low-intensity peaks rise up at 190 and 288 cm^{-1}, for armchair and zigzag nanotubes, respectively, and are assigned to the stretching of the Zn−N bond (Figures 4c and 5c).

Above 700 cm^{-1}, ZnONTs are silent, and the signals due to N−H bonds can be accurately detected. The frequencies calculated for the NH_3 isolated molecule are 1226, 1720 (bending), 3340, and 3443 cm^{-1} (stretching) and result in good agreement with both experimental values[41] and recently computed modes.[42] After adsorption, the two signals at high frequency remain almost unchanged, as expected. On the contrary, the soft bending modes active at lower frequencies, which yield the molecule closer to the ZnONTs, are lowered and split into a few clear signals emerging in the region around 1170 and 1700 cm^{-1}, respectively.

Finally, the topological analysis of the electron density was performed with particular attention to the atoms involved in the ZnONT−NH_3 interaction, represented for sake of clarity in the inset of Figure 6. Results in terms of bond critical points (BCP), their topological properties, and charge densities are collected in Tables 3 and 4. On the basis of the topological indicators,[43] a tentative classification of the various interaction is proposed. The Zn−O bond, as already studied,[33] can be seen as a transit (t) interaction, i.e., neither ionic either covalent. The Zn−N bond can also be placed in the transit region; the driving force in this case seems to be the electrostatic interaction between NH_3 permanent dipole moment with the

DOI: 10.1021/acs.jpcc.6b10396
J. Phys. Chem. C 2017, 121, 8109−8119

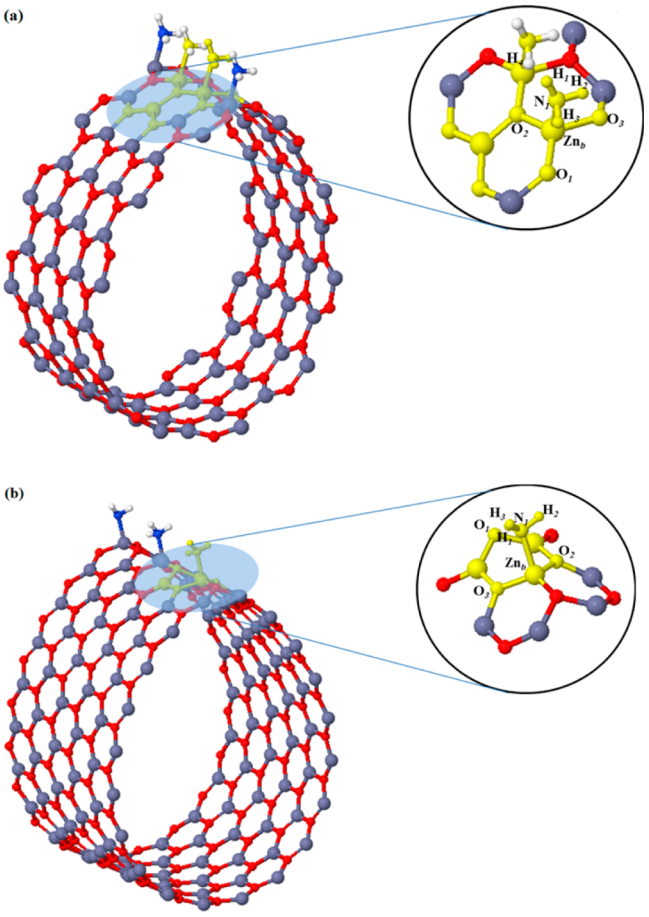

Figure 6. ZnO nanotube with NH_3 molecules adsorbed (a) armchair and (b) zigzag. Yellow denotes atoms that were considered for the topological analysis in Tables 3 and 4.

Zn Lewis acid site. The value of the dipole moment increases as NH_3 approaches the nanotube as demonstrated by the remarkable charge transfer from the protons to the nitrogen. On the contrary, a not appreciable charge transfer is calculated between the two interacting moieties, in particular Zn and O atoms keep both their volume and charge after the adsorption. Hydrogen bonds between NH_3 molecules along the same row are formed on armchair nanotube adsorption, with one proton of each molecule pointing toward the N of the opposite ammonia, and these interactions stabilize the whole structure. In zigzag nanotube, as mentioned, there is an interaction between ammonia H and O nanotube site, characterized as a van der Waals interaction.

In Figures 7 and 8, the total electron density and its Laplacian are shown in the plane containing the Zn−N bond. ZnO charge density is not significantly altered by the adsorption, whereas its geometrical structures is very responsive. On the contrary, NH_3 molecules retain almost the same geometry as in the gas phase but undergo sensitive changes in their electronic features.

On the basis of our results, it is possible to affirm that in the presence of a continuous source of NH_3 the adsorption can proceed until complete coverage of the Zn atoms. Ammonia uptake induces in the ZnONTs structural modifications, which do not however change the fundamental electronic structure, and the overall process is self-catalyzed thanks to the formation of attractive interactions between the adsorbed molecules.

CONCLUSIONS

Periodic DFT calculations with B3LYP and all-electron Gaussian basis set were performed to simulate the structural, electronic, vibrational, and topological properties NH_3 adsorption on armchair and zigzag ZnONTs. The analysis of total energy of the system showed that the NH_3 is adsorbed on

Table 3. Topological Properties of Armchair (10, 10) at the Bond Critical Points Plus Bader Charges and Atomic Volumes (All in Atomic Units) Computed for the Atoms Involved in the Physisorption[a]

	bond critical points								atomic properties	
	$d_{BCP-Zn/N}$	$d_{BCP-O/H}$	$\rho(r)$	$\nabla^2\rho$	$\lvert V\rvert/G$	$H/\rho(r)$	ε	bond	Q	V
Zn_f									1.27	79.80
O_{in}	0.919	0.970	0.098	0.571	1.06	−0.09	0.028	t	−1.12	112.67
O_{out}	0.920	0.971	0.090	0.508	1.05	−0.08	0.028	t	−1.20	111.58
N_f									−0.84	94.36
H_f	0.747	0.279	0.320	−1.359	8.36	−1.23	0.037	cov	0.28	38.83
					1-row NH_3					
Zn_b									1.29	78.93
O_1	0.922	0.975	0.098	0.573	1.06	−0.09	0.026	t	−1.11	111.82
O_2	0.972	0.983	0.095	0.551	1.06	−0.09	0.025	t	−1.19	111.38
O_3	0.941	1.004	0.088	0.489	1.05	−0.08	0.011	t	−1.04	108.96
N_1	1.104	1.197	0.043	0.121	1.23	−0.21	0.034	t	−1.08	111.84
N_1									−1.08	112.83
H_1	0.748	0.279	0.323	−1.413	9.01	−1.25	0.028	cov	0.34	32.40
H_2	0.756	0.267	0.323	−1.454	9.73	−1.27	0.027	cov	0.38	29.90
H_3	0.760	0.263	0.323	−1.472	9.97	−1.28	0.025	cov	0.40	23.11
H_4	1.479	0.880	0.013	0.045	0.91	0.07	0.193	H-bond	0.38	37.71
					10-row NH_3					
Zn_b									1.29	80.58
O_1	0.928	0.984	0.094	0.547	1.06	−0.09	0.021	t	−1.12	112.94
O_2	0.923	0.976	0.097	0.569	1.06	−0,09	0,023	t	−1.20	111.38
O_3	0.936	0.997	0.090	0.509	1.05	−0.08	0.013	t	−1.04	108.98
N_1	1.146	1.236	0.036	0.095	1.25	−0.22	0.041	t	−1.08	114.03
N_1									−1.08	114.03

DOI: 10.1021/acs.jpcc.6b10396
J. Phys. Chem. C 2017, 121, 8109−8119

Table 3. continued

	bond critical points								atomic properties	
	$d_{BCP-Zn/N}$	$d_{BCP-O/H}$	$\rho(r)$	$\nabla^2\rho$	$\lvert V\rvert/G$	$H/\rho(r)$	ε	bond	Q	V
					10-row NH_3					
H_1	0.746	0.276	0.323	1.391	8.71	−1.24	0.030	cov	0.33	33.44
H_2	0.762	0.264	0.321	1.457	9.94	−1.28	0.026	cov	0.40	23.36
H_3	0.755	0.268	0.323	1.440	9.52	−1.26	0.028	cov	0.37	30.51
H_4	1.495	0.892	0.013	0.043	0.91	0.07	0.156	H-bond	0.36	38.26

[a]Bond critical points (electron charge density ($\rho(r)$), Laplacian ($\nabla^2\rho$), $\lvert V\rvert/G$ ratio, bond degree $H/\rho(r)$, and ellipticity ε). Labels of atoms are those in Figure 6. Subindex f refers to the isolated nanotube and NH_3; t, cov, and H-bond refer to transit, covalent, and hydrogen bonds.

Table 4. Topological Properties of Zigzag (20, 0) at the Bond Critical Points Plus Bader Charges and Atomic Volumes (All in Atomic Units) Computed for the Atoms Involved in the Physisorption[a]

	bond critical points								atomic properties	
	$d_{BCP-Zn/H}$	$d_{BCP-O/N}$	$\rho(r)$	$\nabla^2\rho$	$\lvert V\rvert/G$	$H/\rho(r)$	ε	bond	Q	V
Zn_f									1.27	82.89
O_{in}	0.919	0.970	0.099	0.589	1.06	−0.09	0.028	t	−1.15	113.90
O_{out}	0.919	0.971	0.099	0.587	1.06	−0.09	0.028	t	−1.27	115.46
N_f									−0.84	94.36
H_f	0.747	0.279	0.320	−1.359	8.36	−1.23	0.037	cov	0.28	38.83
					1-row NH_3					
Zn_b									1.29	78.90
O_1	0.913	0.962	0.103	0.616	1.06	−0.11	0.027	t	−1.07	108.11
O_2	0.920	0.973	0.098	0.583	1.06	−0.09	0.028	t	−1.09	109.23
O_3	0.921	0.973	0.098	0.581	1.06	−0.09	0.028	t	−1.11	110.89
N_1	1.041	1.143	0.0571	0.183	1.18	−0.17	0.024	t	−1.07	109.10
N_1									−1.07	109.10
H_1	0.272	0.750	0.324	−1.439	9.49	−1.26	0.026	cov	0.350	30.43
H_2	0.270	0.751	0.325	−1.448	9.59	−1.26	0.026	cov	0.355	31.10
H_3	0.263	0.768	0.316	−1.42	10.18	−1.26	0.024	cov	0.419	22.55
H_3									0.419	22.55
O_1	0.845	1.443	0.014	0.049	0.89	0.09	0.042	VDW	−1.11	80.50
					10-row NH_3					
Zn_b									1.29	79.72
O_1	0.911	0.959	0.104	0.628	1.06	−0.11	0.028	t	−1.09	109.69
O_2	0.920	0.973	0.098	0.587	1.06	−0.09	0.029	t	−1.10	109.80
O_3	0.917	0.967	0.101	0.598	1.06	−0.10	0.027	t	−1.13	111.07
N_1	1.051	1.153	0.054	0.170	1.11	−0.18	0.028	t	−1.07	110.87
N_1									−1.07	110.87
H_1	0.273	0.748	0.324	−1.43	9.34	−1.25	0.027	cov	0.348	31.56
H_2	0.274	0.749	0.324	−1.44	9.35	−1.26	0.027	cov	0.353	31.55
H_3	0.262	0.773	0.311	−1.39	10.02	−1.26	0.024	cov	0.417	22.78
H_3									0.417	22.78
O_1	0.777	1.357	0.019	0.069	0.93	0.05	0.044	VDW	−1.09	79.72

[a]Bond critical points (electron charge density ($\rho(r)$), Laplacian ($\nabla^2\rho$), $\lvert V\rvert/G$ ratio, bond degree $H/\rho(r)$, and ellipticity ε). Labels of atoms are as in Figure 6. Subindex f refers to the isolated nanotube and NH_3; t, cov, H-bond, and VDW refer to transit, covalent, hydrogen, and van der Waals bond typea.

Zn and that the interaction between the polar molecule and the basic site plays a leading role in determining the adsorption energy of the system.

The band structure of the host ZnONTs system is practically unchanged, and only few differences in the Zn atoms 3d orbitals contributing to the valence bands were appreciated. NH_3−ZnONTs interaction produces its traces in the IR spectrum where Zn−N vibrational modes appear around 190 and 288 cm^{-1}, for armchair and zigzag nanotubes, respectively, and the frequencies of the isolated systems are perturbed by the adsorption. The onset of a Zn−N interaction and the formation of N···H hydrogen bond and van der Waals interaction were also confirmed by the topological analysis of the electron density.

With an increase of molecules adsorbed, the deformation at nanotube structure decreases, and weak attractive interactions between adsorbed molecules are evaluated. Then, it can be concluded that in a real system the molecules trend to saturated the surface and not significantly change the nanotube structure or the semiconductor character as the energy band gap is preserved.

The results confirm that the ammonia is adsorbed on ZnO nanotubes via Zn atoms, characterized as a physisorption and not a chemisorption, as there are no changes on the nanotube charges and electronic structure. In gas sensors, the physisorption is important due to the ease of desorption under appropriate conditions, in order to regenerate the substrate (in this case, the nanotube). On the basis of the results obtained

DOI: 10.1021/acs.jpcc.6b10396
J. Phys. Chem. C 2017, 121, 8109−8119

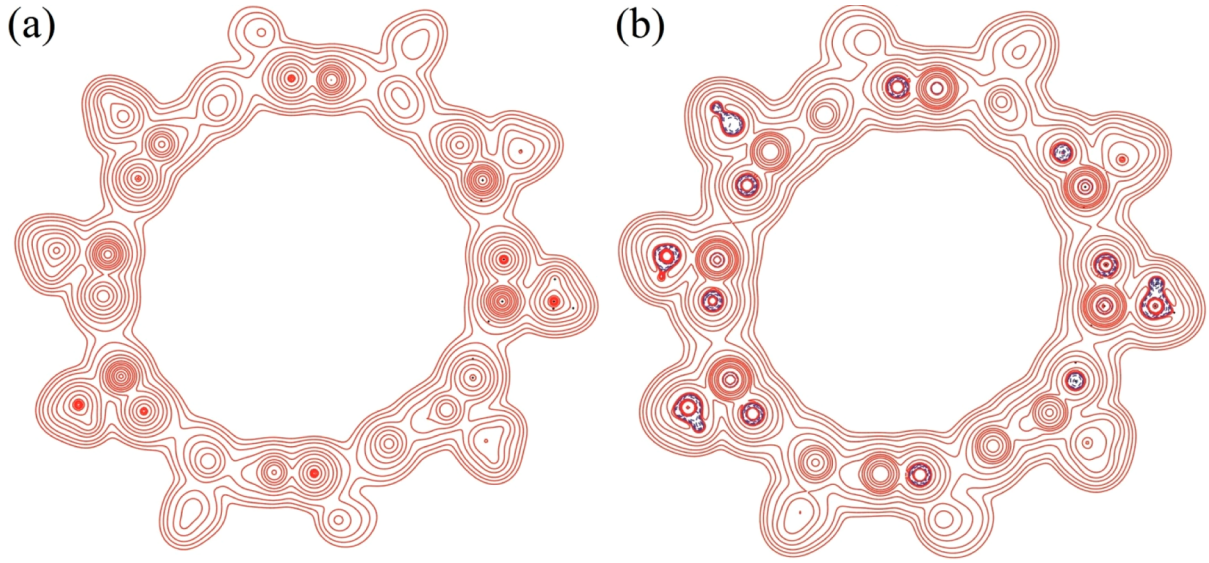

Figure 7. *10*NH_3@ZnONT (10, 10). (a) Electron density and (b) Laplacian of the electron density in the plane containing the N−Zn−O atoms. A logarithmic scale is adopted between −0.1 and 0.1 au. Continuous red and dotted blue lines indicate positive and negative contour levels, respectively.

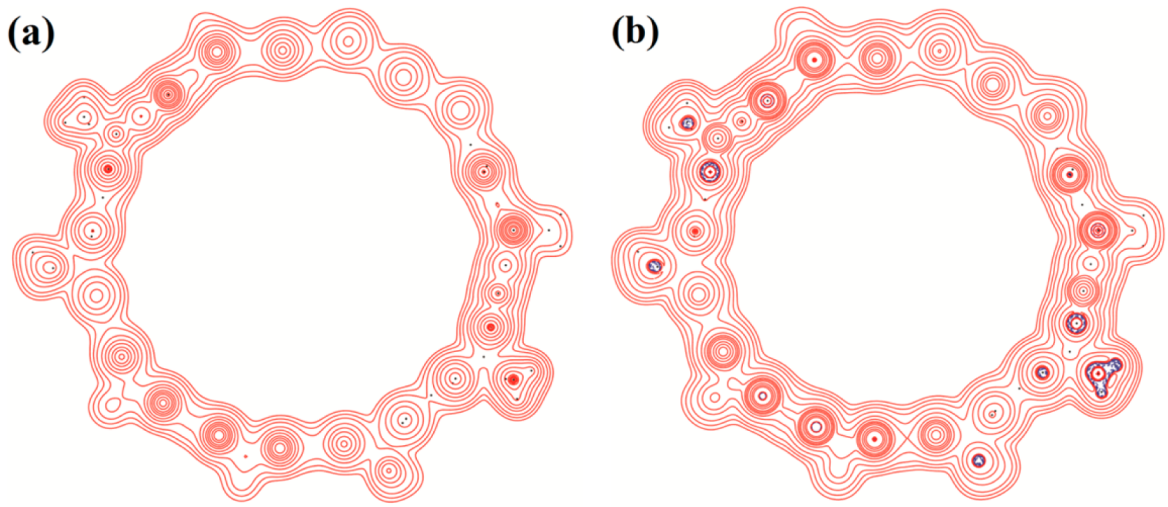

Figure 8. *10*NH_3@ZnONT (20, 0). (a) Electron density and (b) Laplacian of the electron density in the plane containing the N−Zn−O atoms. A logarithmic scale is adopted between −0.1 and 0.1 au. Continuous red and dotted blue lines indicate positive and negative contour levels, respectively.

for Zn−N bond length, adsorption energy, topological analysis, and infrared spectra, the ZnONTs can be a potential gas sensor.

■ ASSOCIATED CONTENT

Supporting Information

The Supporting Information is available free of charge on the ACS Publications website at DOI: 10.1021/acs.jpcc.6b10396.

Models of adsorption site, single-molecule adsorption, all models of NH_3 adsorption on armchair and zigzag nanotubes, and band structure of bare nanotube and saturated nanotube (PDF)

■ AUTHOR INFORMATION

Corresponding Author

*E-mail: sambrano@fc.unesp.br.

ORCID

Julio R. Sambrano: 0000-0002-5217-7145

Notes

The authors declare no competing financial interest.

■ ACKNOWLEDGMENTS

This work is supported by Brazilian Funding Agencies: CNPq (46126-4), CAPES PROCAD (88881068492/2014-01), and FAPESP (2013/19713-7, 2013/07296-2, 2016/07954-8, and 2016/07476-9). The computational facilities were supported by resources supplied by Molecular Simulations Laboratory, São Paulo State University, Bauru, Brazil. Special thanks to the Theoretical Group of Chemistry, Torino University.

■ REFERENCES

(1) Reynolds, D. C.; Look, D. C.; Jogai, B. Optically pumped ultraviolet lasing from ZnO. *Solid State Commun.* **1996**, *99*, 873−875.
(2) Ozgur, U.; Hofstetter, D.; Morkoc, H. ZnO Devices and Applications: A Review of Current Status and Future Prospects. *Proc. IEEE* **2010**, *98*, 1255−1268.

DOI: 10.1021/acs.jpcc.6b10396
J. Phys. Chem. C 2017, 121, 8109−8119

(3) Morkoç, H.; Özgür, Ü. *Zinc Oxide: Fundamentals, Materials and Device Technology*; Wiley-VHC: Weinheim, Germany, 2009.
(4) Catto, A. C.; da Silva, L. F.; Ribeiro, C.; Bernardini, S.; Aguir, K.; Longo, E.; Mastelaro, V. R. An easy method of preparing ozone gas sensors based on ZnO nanorods. *RSC Adv.* **2015**, *5*, 19528−19533.
(5) Rocha, L. S. R.; Foschini, C. R.; Silva, C. C.; Longo, E.; Simões, A. Z. Novel ozone gas sensor based on ZnO nanostructures grown by the microwave-assisted hydrothermal route. *Ceram. Int.* **2016**, *42*, 4539−4545.
(6) Biasotto, G.; Ranieri, M. G. A.; Foschini, C. R.; Simões, A. Z.; Longo, E.; Zaghete, M. A. Gas sensor applications of zinc oxide thin film grown by the polymeric precursor method. *Ceram. Int.* **2014**, *40*, 14991−14996.
(7) Wang, X. M.; Sun, F. Z.; Duan, Y. Q.; Yin, Z. P.; Luo, W.; Huang, Y. A.; Chen, J. K. Highly sensitive, temperature-dependent gas sensor based on hierarchical ZnO nanorod arrays. *J. Mater. Chem. C* **2015**, *3*, 11397−11405.
(8) Chen, T.-Y.; Chen, H.-I.; Hsu, C.-S.; Huang, C.-C.; Wu, J.-S.; Chou, P.-C.; Liu, W.-C. Characteristics of ZnO nanorods-based ammonia gas sensors with a cross-linked configuration. *Sens. Actuators, B* **2015**, *221*, 491−498.
(9) Wan, Q.; Li, Q. H.; Chen, Y. J.; Wang, T. H.; He, X. L.; Li, J. P.; Lin, C. L. Fabrication and ethanol sensing characteristics of ZnO nanowire gas sensors. *Appl. Phys. Lett.* **2004**, *84*, 3654−3656.
(10) Wang, X. H.; Zhang, J.; Zhu, Z. Q. Ammonia sensing characteristics of ZnO nanowires studied by quartz crystal microbalance. *Appl. Surf. Sci.* **2006**, *252*, 2404−2411.
(11) An, W.; Wu, X.; Zeng, X. C. Adsorption of O-2, H-2, CO, NH3, and NO2 on ZnO nanotube: A density functional theory study. *J. Phys. Chem. C* **2008**, *112*, 5747−5755.
(12) Gangopadhyay, R. K.; Das, S. K. Ammonia leakage from refrigeration plant and the management practice. *Process Saf. Prog.* **2008**, *27*, 15−20.
(13) Saito, S.; Miyayama, M.; Koumoto, K.; Yanagida, H. Gas sensing characteristic of porous ZnO and Pt/ZnO ceramics. *J. Am. Ceram. Soc.* **1985**, *68*, 40−43.
(14) Nanto, H.; Minami, T.; Takata, S. Zinc-oxide thin-film ammonia gas sensors with high-sensitivity and excellent selectivity. *J. Appl. Phys.* **1986**, *60*, 482−484.
(15) Aslam, M.; Chaudhary, V. A.; Mulla, I. S.; Sainkar, S. R.; Mandale, A. B.; Belhekar, A. A.; Vijayamohanan, K. A highly selective ammonia gas sensor using surface-ruthenated zinc oxide. *Sens. Actuators, A* **1999**, *75*, 162−167.
(16) Bader, R. F. W. *Atoms in Molecules−A Quantum Theory*; Oxford University Press: Oxford, U. K., 1990.
(17) Dovesi, R.; Orlando, R.; Erba, A.; Zicovich-Wilson, C. M.; Civalleri, B.; Casassa, S.; Maschio, L.; Ferrabone, M.; De La Pierre, M.; D'Arco, P.; et al. CRYSTAL14: A Program for the Ab Initio Investigation of Crystalline Solids. *Int. J. Quantum Chem.* **2014**, *114*, 1287−1317.
(18) Maul, J.; Santos, I. M. G.; Sambrano, J. R.; Erba, A. Thermal properties of the orthorhombic CaSnO3 perovskite under pressure from ab initio quasi-harmonic calculations. *Theor. Chem. Acc.* **2016**, *135*, 36.
(19) Albuquerque, A. R.; Maul, J.; Longo, E.; dos Santos, I. M. G.; Sambrano, J. R. Hydrostatic and 001 Uniaxial Pressure on Anatase TiO2 by Periodic B3LYP-D* Calculations. *J. Phys. Chem. C* **2013**, *117*, 7050−7061.
(20) Duarte, T. M.; Buzolin, P. G. C.; Santos, I. M. G.; Longo, E.; Sambrano, J. R. Choice of hybrid functional and basis set optimization to calculate the structural, electronic, mechanical, and vibrational properties of BaSnO3. *Theor. Chem. Acc.* **2016**, *135*, 151.
(21) Becke, A. D. Density-functional Thermochemistry 0.3. The Role of Exact Exchange. *J. Chem. Phys.* **1993**, *98*, 5648−5652.
(22) Lee, C. T.; Yang, W. T.; Parr, R. G. Development of the colle-salvetti correlation-energy formla into a functional of the electron-density. *Phys. Rev. B: Condens. Matter Mater. Phys.* **1988**, *37*, 785−789.
(23) Dovesi, R.; Roetti, C.; Orlando, R.; Zicovich-Wilson, C. M.; Pascale, F.; Civalleri, B.; Doll, K.; Harrison, N. M.; Bush, I. J.; D'Arco, P.; et al. *CRYSTAL14 User's Manual*: University of Torino: Torino, Italy, 2014.
(24) Jaffe, J. E.; Hess, A. C. Hartree-Fock study of Phase-changes in ZnO at High-pressure. *Phys. Rev. B: Condens. Matter Mater. Phys.* **1993**, *48*, 7903−7909.
(25) Bredow, T.; Jug, K.; Evarestov, R. A. Electronic and magnetic structure of ScMnO3. *Phys. Status Solidi B* **2006**, *243*, R10−R12.
(26) Dovesi, R.; Causa', M.; Orlando, R.; Roetti, C.; Saunders, V. R. Abinitio approach to molecular-crystals - A periodic Hartree-Fock study of crystalline urea. *J. Chem. Phys.* **1990**, *92*, 7402−7411.
(27) Dovesi, R.; Ermondi, E.; Ferrero, E.; Pisani, C.; Roetti, C. Hartree-Fock study of lithium hydride with the use of a polarizable basis set. *Phys. Rev. B: Condens. Matter Mater. Phys.* **1984**, *29*, 3591−3600.
(28) Gatti, C.; Casassa, S. *TOPOND user's manual*; CNR-ISTM: Milano, Italy, 2014. http://www.crystal.unito.it/topond/topond.pdf.
(29) Pascale, F.; Zicovich-Wilson, C. M.; López Gejo, F.; Civalleri, B.; Orlando, R.; Dovesi, R. The calculation of the vibrational frequencies of crystalline compounds and its implementation in the CRYSTAL code. *J. Comput. Chem.* **2004**, *25*, 888−897.
(30) Zicovich-Wilson, C. M.; Pascale, F.; Roetti, C.; Saunders, V. R.; Orlando, R.; Dovesi, R. Calculation of the vibration frequencies of alpha-quartz: The effect of Hamiltonian and basis set. *J. Comput. Chem.* **2004**, *25*, 1873−1881.
(31) Noel, Y.; D'Arco, P.; Demichelis, R.; Zicovich-Wilson, C. M.; Dovesi, R. On the Use of Symmetry in the Ab Initio Quantum Mechanical Simulation of Nanotubes and Related Materials. *J. Comput. Chem.* **2009**, *31*, 855−862.
(32) Marana, N. L.; Albuquerque, A. R.; La Porta, F. A.; Longo, E.; Sambrano, J. R. Periodic density functional theory study of structural and electronic properties of single-walled zinc oxide and carbon nanotubes. *J. Solid State Chem.* **2016**, *237*, 36−47.
(33) Marana, N. L.; Casassa, S. M.; Longo, E.; Sambrano, J. R. Structural, Electronic, Vibrational and Topological Analysis of Single-Walled Zinc Oxide Nanotubes. *J. Phys. Chem. C* **2016**, *120*, 6814−6823.
(34) Vanduijneveldt, F. B.; Vanduijneveldtvanderijdt, J.; Vanlenthe, J. H. Statue-of-the-art in counterpoise theory. *Chem. Rev.* **1994**, *94*, 1873−1885.
(35) Mayer, I.; Valiron, P. Second order M?ller-Plesset perturbation theory without basis set superposition error. *J. Chem. Phys.* **1998**, *109*, 3360−3373.
(36) Casarin, M.; Maccato, C.; Vittadini, A. A comparative study of the NH3 chemisorption on ZnO(1010) and Cu2O(111) non-polar surfaces. *Chem. Phys. Lett.* **1999**, *300*, 403−408.
(37) Casarin, M.; Tondello, E.; Vittadini, A. A LCAO-LDF study of CO and NH3 chemisorption on ZnO(0001). *Surf. Sci.* **1994**, *307-309*, 1182−1187.
(38) Casarin, M.; Tondello, E.; Vittadini, A. Coordination chemistry of CO and NH3 on ZnO(0001) - A molecular cluster study of the CO and NH3 bonding interaction with d10 ion. *Surf. Sci.* **1994**, *303*, 125−138.
(39) Lopes Martins, J. B.; Longo, E.; Rodríguez Salmon, O. D.; Espinoza, V. A. A.; Taft, C. A. The interaction of H-2, CO, CO2, H2O and NH3 on ZnO surfaces: an Oniom Study. *Chem. Phys. Lett.* **2004**, *400*, 481−486.
(40) Lima, R. C.; Macario, L. R.; Espinosa, J. W. M.; Longo, V. M.; Erlo, R.; Marana, N. L.; Sambrano, J. R.; dos Santos, M. L.; Moura, A. P.; Pizani, P. S.; Andres, J.; Longo, E.; Varela, J. A. Toward an understanding of intermediate- and short-range defects in ZnO single crystals. A combined experimental and theoretical study. *J. Phys. Chem. A* **2008**, *112*, 8970−8978.
(41) Morimoto, T.; Yanai, H.; Nagao, M. Infrared spectra of ammonia adsorbed on zinc oxide. *J. Phys. Chem.* **1976**, *80*, 471−475.
(42) Alecu, I. M.; Zheng, J. J.; Zhao, Y.; Truhlar, D. G. Computational Thermochemistry: Scale Factor Databases and Scale Factors for Vibrational Frequencies Obtained from Electronic Model Chemistries. *J. Chem. Theory Comput.* **2010**, *6*, 2872−2887.
(43) Gatti, C. Chemical bonding in crystals: new directions. *Z. Kristallogr. - Cryst. Mater.* **2005**, *220*, 399−457.

DOI: 10.1021/acs.jpcc.6b10396
J. Phys. Chem. C 2017, 121, 8109−8119